JOURNAL OF IMAGING SCIENCE AND TECHNOLOGY® • Volume 49, Number 4, July/August 2005

Optical Properties of Nanoparticulate Metallic Silver in Photothermographic Imaging Materials

D. R. Whitcomb▲
Eastman Kodak Company, Oakdale, Minnesota, USA

S. Chen, J. D. Shore and P. J. Cowdery-Corvan
Eastman Kodak Company, Rochester, New York, USA

K. A. Dunn
University at Albany, SUNY, Albany, New York, USA

The fundamental building blocks of light absorption in photothermographic imaging systems are the nanosized silver particles formed from the thermally induced reduction of silver ions. The silver particles tend to be filaments or clustered agglomerations of nanospheres (dendrites). While the silver particle size is well known to be important for light absorption properties, it is shown here that the physical proximity between particles is also a critical controlling factor in obtaining a neutral black image tone. It is further shown that the ideal form of metallic silver in any thermally developed black and white imaging system comprises dispersed, tight (physically separated by 0–30 Å) clusters of 10–30 polydisperse, spherical silver nanoparticles, each having diameters in the 5–30 nm range. The minimum cluster aggregation size should be in the 50–200 nm diameter range, depending on shape. This understanding provides a target for silver efficiency, tone, and optical density for photothermographic media constructions.

Journal of Imaging Science and Technology 49: 370–380 (2005)

Introduction

Conventional black and white silver halide photographic films use the reduction of silver halide to metallic silver to generate a light absorbing component.[1] Ideally, the metallic silver absorbs light uniformly throughout the visible spectrum in order to achieve a neutral black image. The ability of the silver to achieve this color, however, is directly related to multiple properties of the metallic silver deposit, including size, shape, morphology, concentration, and relative juxtaposition between silver particles. The normal size and shape of the silver in conventional silver halide-based photographic products are filamentary,[1] as shown in Fig. 1. This form of chemically developed silver is the most prevalent form seen in most photographic films. It can appear either as isolated silver slivers or as entwined "steel wool" bundles, a shape that would modify its overall light absorption and tone properties.[1] Changes in silver filament size associated with tone changes in black-and-white photographic films have also been documented.[2]

Black-and-white photothermographic (PTG) materials can be viewed, at least superficially, to be based on conventional silver halide chemistry.[3–6] However, as close inspection reveals, there are a multitude of differences that make direct comparisons between the two difficult.[7,8] For example, while Ag^+ is reduced to silver in both cases, the source of the silver ions is quite different, thereby requiring different chemistries to efficiently convert the ion to metal. In addition, development time and temperature profiles are significantly different, not to mention the presence or absence of solvent. Furthermore, while some information is being published regarding the metallic silver in photothermographic systems, [9–12] the properties of the metallic silver that are optimum for proper color tone and silver usage efficiency in these systems are not well established.

In determining the metallic silver properties that control optical density and image tone in any B&W thermally developed film, it is clear that the formulation and imaging differences between thermographic (TG) and PTG imaging constructions will be important factors. First, it must be recognized that the development time-temperature regimes are different by orders of magnitude. For example, the thermal processing of

---

Original manuscript received January 6, 2005

▲ IS&T Member

Corresponding Author: D. R. Whitcomb, David.whitcomb@ kodak.com

TABLE I. Toners and Developers for TG and PTG Imaging Formulations

Function	Thermographic	Photothermographic
Developer	3,4-dihydroxybenzoic acid 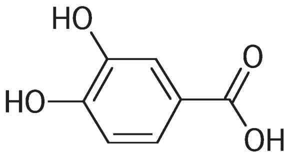	Lowinox 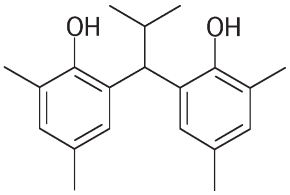
Toner	benzoxazinedione 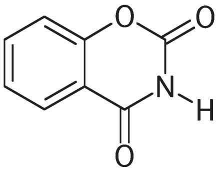 or phthalazinone 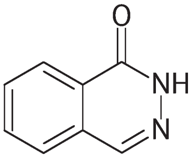	PA 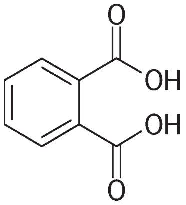 or PHZ 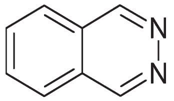

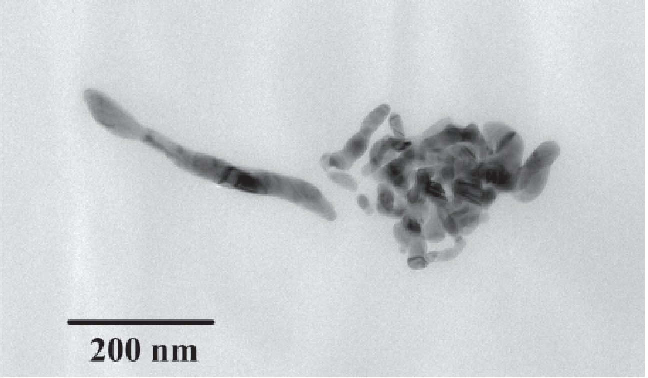

Figure 1. Transmission electron microscopy (TEM) image of filamentary silver in Kodak Electron Microscope Film 4489, a conventional black-and-white (B&W) photographic product.

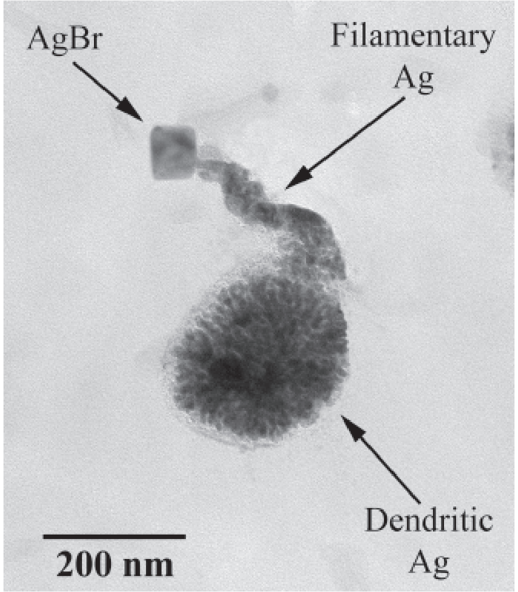

Figure 2. Typical silver in PTG imaging materials.

current PTG materials proceeds at ~120°C over the course of 15 seconds, while a thermal printhead produces intense heat (~350–400°C) thermal pulses in a 5–20 ms timeframe.[13,14] The toners and developers, therefore, must be chosen for optimum operation under the selected conditions. The optimum silver sources for the current developer/toner technology tends to be silver carboxylates (salts of long chain fatty acids, such as stearic, C_{18}, arachidic, C_{20}, and behenic, C_{22}) in both cases, but the toners and developers in these formulations are quite different. For example, TG formulations utilize highly reactive catechol derivatives, such as 3,4-dihydroxybenzoic acid,[15] as developers, compared to the less reactive bis-phenols, such as Lowinox™, in PTG formulations. At the same time, TG formulations include benzoxazinedione or phthalazinone for the toner, while the phthalazine/phthalic acid combination is used for PTG constructions,[3,4] Table I.

It is known that the microscopic image forming element in PTG imaging materials, coated from organic solvents, is a combination of different metallic silver particles[16] made up of the well-recognized filamentary shape of conventional photographic films coupled to a unique "dendritic" silver. The latter is characterized by a composition of extremely fine silver nanoparticles (2–10 nm diameter) tightly clustered together in a roughly spherical, aggregated shape (~0.2 µm diameter), Fig. 2.

The unique dendritic silver, which develops at the end of the filamentary silver, has a grape cluster-like morphology and contains a collection of nanoparticles in close proximity to each other. This morphology provides a much higher surface area-to-volume ratio than that of filamentary silver.

Because of time-temperature and toner-developer differences, the silver deposit formed in TG imaging materials tends to be agglomerations of spherical nanoparticulate silver (5–30 nm diameter range) observed to cluster together to form linear aggregates (~0.2–1 µm long) that give a reasonably neutral black image, such as in the Agfa DRYSTAR film, Fig. 3.

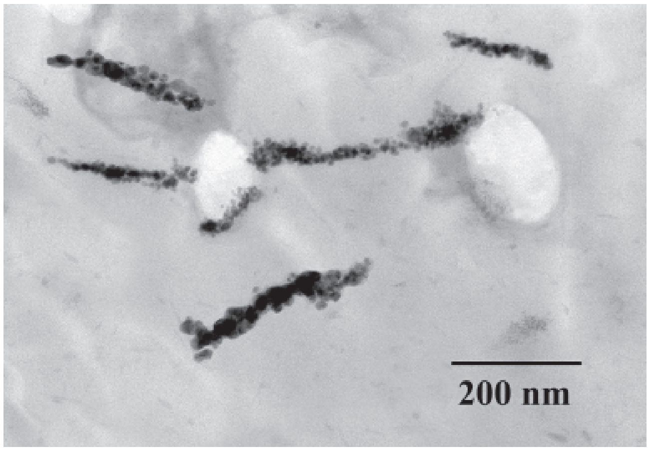

Figure 3. Silver agglomerations in TG imaging materials, Drystar™.

The objective of this report is to correlate silver physical properties (size, shape, morphology, concentration, juxtaposition) to optical properties, and, especially, to demonstrate how agglomeration of particles changes the light absorption spectrum from peaking in the blue part of the spectrum, for isolated silver nanoparticles, to being panchromatic for larger agglomerations of particles. In addition, we shall predict how these properties apply to PTG systems based on thermally generated silver.

Experimental

Transmission Electron Microscopy (TEM)

Microstructures of imaged films were examined via their TEM cross sections using a JEM 2000FX electron microscope operating at 200 kV accelerating voltage. Cooling the sample to a nominal temperature of –180°C minimized electron beam induced silver printout. Details of the fine features were resolved by high resolution imaging conditions, and composition analysis was carried out by energy dispersive spectroscopy (EDS) with the electron beam focused to areas as small as 5 nm. Thin sections were prepared by microtomy, using a diamond knife, and floated off on water onto Formvar coated Cu grids. High resolution lattice images were captured in a JEM 2010F electron microscope fitted with an ultra-narrow gap pole piece, capable of 0.18 nm point-to-point resolution.

Ultraviolet/Visible (UV/VIS) Spectroscopy

The absorption spectra of colored films were taken in a double beam instrument (PerkinElmer Lambda 2), using an unprocessed, blue-base film in the reference beam, and represented the preferred method to quantify their color variations.

Preparation of Carey Lea Silver, CLS (Allotropic Form of Silver A).[17]

Three solutions were prepared:

- 8.0 g Ferrous ammonium sulfate in 15 g H_2O
- 7.01 g NaOH and 11.2 g citric acid (Aldrich) in 15 g H_2O, both of which were dissolved in portions (NaOH first) to avoid overheating. These amounts correspond to 3:1 NaOH:citric acid.
- 2.1 g $AgNO_3$ dissolved in 20 g H_2O. Note that the reagents correspond to large molar excesses, relative to Ag^+, i.e., 15:58:11 mmol Fe^{++}:citric acid:Ag^+

The trisodium citrate solution is added to the ferrous ammonium sulfate solution and stirred about 1 min. This lightly colored solution (pale green) is poured into the silver nitrate solution with rapid stirring. The silver solution is observed to change color and precipitate rapidly, from white to red to purple to black. After 30 min of stirring, the reaction mixture is slowly filtered through 0.2–0.6 μm glass fiber paper. The blue, pasty solid, when added to water, instantly redisperses to a clear, deep blood red dispersion (colloid). Addition of polyvinylpyrrolidinone produces a clear, stable red–brown dispersion (colloid) that can be coated at different thicknesses and concentrations.

Results and Discussion

The results and discussion are divided into two sections:

I. Carey Lea silver – the fundamental building block of the light-absorption component within the dendritic component of the image in PTG imaging systems. Changes in its morphology represent changes to image tone and silver usage efficiency.
II. Computational modeling of light absorption by nanosized metallic silver particles, and the correlation of their physical properties (size, shape, morphology, concentration and relative juxtaposition between them) to image tone.

The results of this work have direct application to the various aspects of light absorption of silver particles in thermally developed imaging materials.

I. Carey Lea Silver (CLS) – Correlation of Particle Size to Light Absorption

In order to systematically investigate the correlation of light absorption by nanosized silver particles with their physical properties, a relatively controlled composition is needed. Systematic studies of the properties of coinage metals in the nanometer size range first began with Faraday's work on gold in 1857.[18] The nature of the product, in terms of size, shape, and morphology, was found to be highly dependent upon the use of the reducing agent, as well as the experimental conditions.[19] The stabilizing nature of citrate anion has been examined by surface enhanced Raman spectroscopy.[20] Faraday's colloidal gold was recently characterized by TEM to consist of a polydispersed mixture of nanoparticles in the 30–300 nm size range.[20]

Reproducible preparation of nanosized silver particles, however, was more difficult, and it was accomplished much later through some very careful work by M. C. Lea,[17] therefore the term "Carey Lea silver" (CLS). Lea prepared an insoluble (in high ionic-strength aqueous solutions) metallic silver powder, which readily redisperses in pure water (low ionic strength), that he referred to as one of three "allotropic" forms of silver. A highly diluted sample of this silver has an excellent bright yellow color, a property that has been utilized by the photographic industry as a blue filter in conventional color negative photographic films.[21] According to the original literature, CLS can be precipitated as a blue–black solid that readily redisperses in pure water to produce yellow, red, and brown solutions. On further dilution, the red solution first becomes orange and then bright yellow. Of particular interest, as shown below, was that coatings from aqueous polyvinylpyrrolidinone (PVP) solutions not only dry to different colors, depending on initial solution concentrations, but the darker reddish–brown colored films can be thermally treated to generate black. These series of observations

Figure 4. Color images of CLS coated in PVP (Photoshop simulations that best represented the transmission color observed). The colors are the result of changes in silver concentration.

were good indications that physical changes were occurring with the nanosized silver particles that could be directly correlated to optical properties.

The surface properties of CLS have been studied by surface-enhanced Raman spectroscopy (SERS), which confirmed Lea's original analysis regarding the possible passivation property of residual citrate, and showed that the nanoparticulate silver is covered by a monolayer of citrate ion from the reduction process.[22] In addition, the carboxylate bands of the citrate in the IR were found to be consistent with monodentate coordination. This surface complexation with an anionic ligand is expected with a surface known to comprise silver ions.[23–25]

Calculation of tone changes in silver-based transfer image systems have suggested that particle aggregation plays a role in changing a brown tone toward black.[26–28] In addition, spherical, more or less, silver particles have been reported as a route to create different color images in "chromogenic imaging" materials.[29–31] In these cases, the particle size was observed to be a major contributor to the image color, although particle shape also played a role. The particle sizes studied were large, typically above 100 nm diameters, quite outside the CLS size range important for thermographic imaging materials, as noted below.

Following the original CLS preparation method, except for the addition of PVP binder, we made a highly dilute and crystal clear yellow CLS (colloidal) solution, which dried to a correspondingly crystal clear, yellow film, Fig. 4(a). With less dilution, a light red solution gave a similarly crystal clear deep red film, Fig. 4(b). More concentrated solutions produced various brown (Fig. 4(c)), black (Fig. 4(d)), and metallic-sheened films. The colors of these films are shown as simulation color patches, made in Photoshop™, Fig. 4. (These simulated patches are shown because direct imaging of the film colors using transmitted light did not produce realistic colors). While the use of these color patch simulations rendered color closer to that of the original film, this property is best quantified by their UV/VIS absorption spectra, Fig. 5.

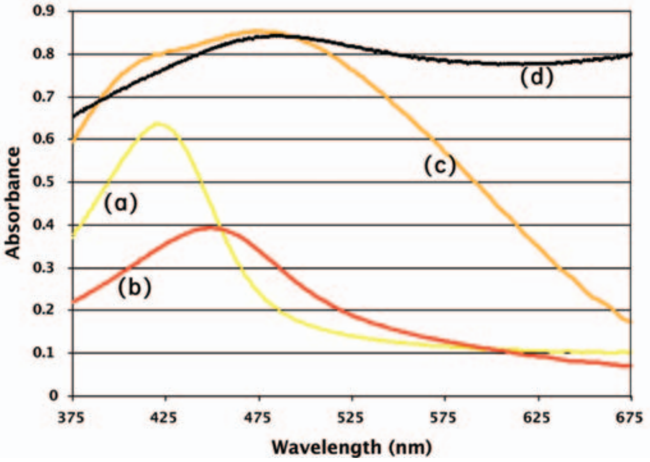

Figure 5. Absorption spectra of colored films prepared from the CLS via the 1889 procedure in Ref. 17 and coated at different concentrations from PVP/water: (a) yellow, (b) red, (c) brown, and (d) black, corresponding to Fig. 4.

For each film, the microstructure of the silver particles was examined by TEM using microtomed cross sections. The yellow film contained a dispersion of isolated, nanoparticulate silver, each spherical in morphology, and polydisperse in size, Fig. 6(a). In the other films, aggregates predominated. In the red film, clusters were small, consisting predominantly of 1–3 nanoparticles, Fig. 6(b), while in the brown film, aggregates were primarily made up of 2–5 nanoparticles, Fig. 6(c). In the black film, aggregate size had a much broader range, consisting of from 3 up to more than 50 nanoparticles, Fig. 6(c). In these, it was possible to discern the component particle size within each aggregate and the size changes among the four films. Clearly the change in film color is accompanied by significant increases in both component as well as aggregate silver size variations, Table II.

Detailed examination of small, spherical silver nanoparticles in the yellow film provided an understanding of the basis for aggregate formation in the other films. A high magnification image of the dispersion showed that the particles are very small and isolated, Fig. 7. High resolution lattice imaging (HRLI) using an ultra-narrow gap pole piece microscope (JEM 2010F) was used to unravel their internal crystal lattice orientation in order to understand the particle growth process. Most particles, particularly the smaller ones (5–15 nm) contained only one crystalline orientation, Fig. 8(a). However, many particles, even those with a spherical shape, contained "polycrystalline" lattice orientations, Fig. 8(b). These particles, 5–30 nm in diameter, represented the smallest and fundamental "building blocks" that form the aggregates found in the other colored CLS films.

High resolution lattice imaging also provided insight into the microstructure of silver aggregates in the red, brown, and black CLS film. While this is discussed further

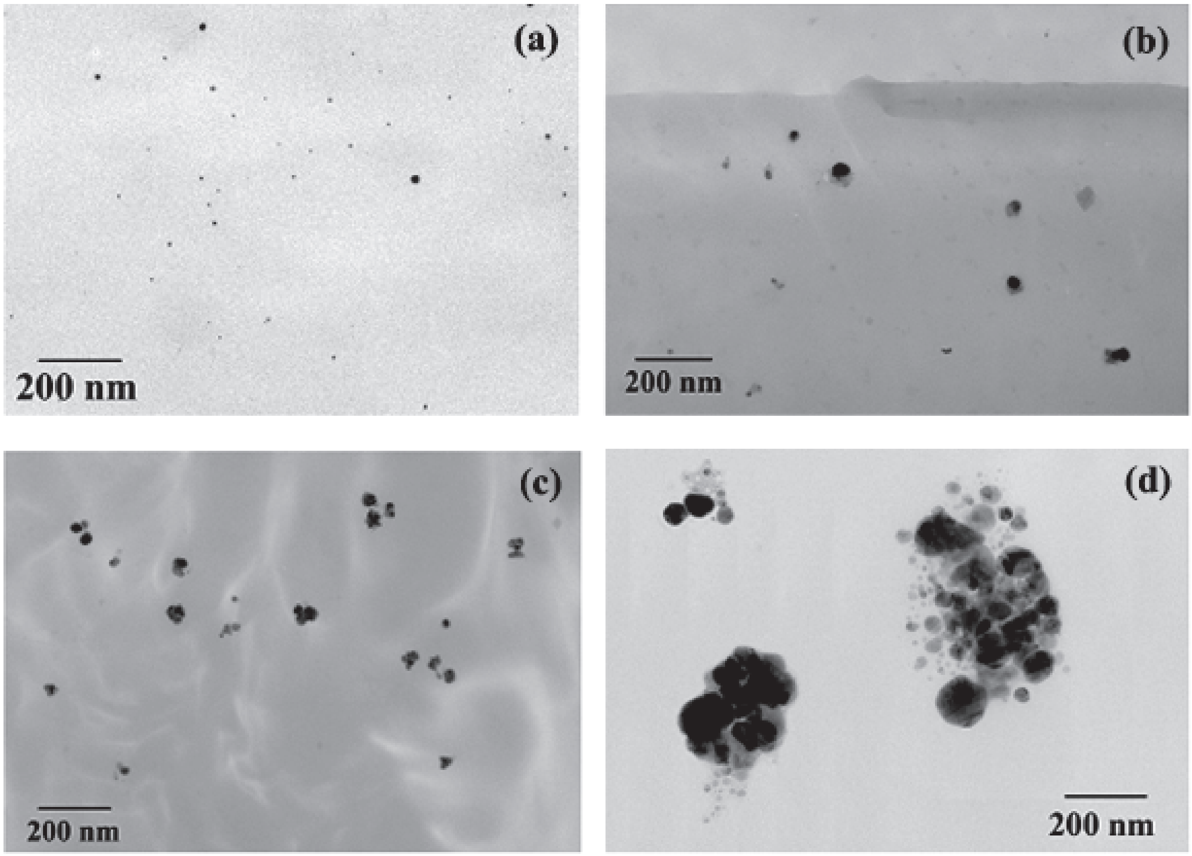

Figure 6. Microstructure of silver in different colored CLS films: yellow (a), red (b), brown (c), black (d), corresponding to Fig. 4.

TABLE II. Diameter of Component and Aggregate Particles in Colored CLS Films

Component	Particle size	Aggregate size
Yellow CLS film	5–30 nm	None
Red CLS film	10–50	20–80 nm
Brown CLS film	10–80	20–250
Black CLS film	20–150	60–500+

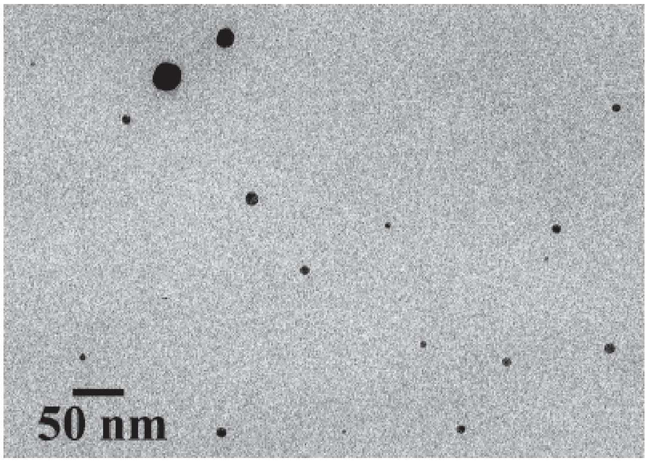

Figure 7. High magnification TEM image of isolated, polydisperse silver particles in the yellow

below, it is noted here that the room temperature, concentration induced change in film tone is accompanied by minimal coalescence of both single and polycrystalline nanoparticles (see Figs. 6(b), (c) and (d)), both which are similar to those described in Figs. 8(a) and (b).

An alternative route to produce a black CLS film was found by heating the brown CLS film to about 200°C for a few seconds. This film contained a high density of large silver clusters, with most ~150–200 nm in diameter, Fig. 9, dispersed in a background of smaller particulates (50–100 nm) that are similar to those seen in the brown CLS, Fig. 6(c). Clearly, heating has caused aggregation, suggesting that these particles have become mobile in the binder and have fused after aggregation. This is not surprising since the water content of the PVP film is sufficiently high that particle mobility can be expected to occur at relatively low temperatures (differential thermal analysis of the film showed phase change transitions occurring beginning at 50°C). The silver particles exhibit morphological differences from those in the concentration induced silver aggregates of Fig. 6(d). They appear significantly more fused, and the component particles are distinctly larger. This thermally induced "condensation" of the silver aggregate is expected to decrease its surface area to volume ratio, as the aggregate changes from an irregular to a near-spherical shape, accompanied by a reduction in aggregate size. It may be noted that a related phenomenon of fusion of aggregated

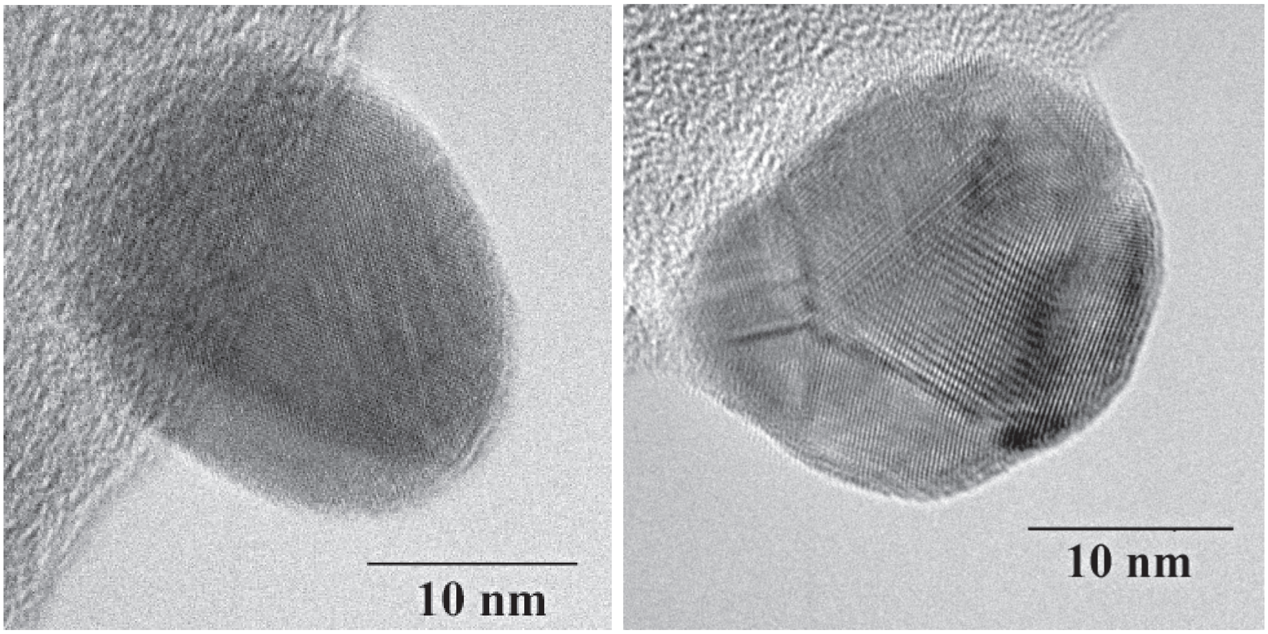

(a) (b)

Figure 8. High resolution lattice image of a silver nanoparticle in the yellow film, showing one set of lattice fringes (a), showing multiple lattice faces (b).

clusters of gold nanoparticles by application of a laser pulse has recently been reported.[32]

This evidence indicates that both the thermally generated and concentration induced aggregates can give neutral tones, even though the latter is composed of individual nanoparticles, each which, by itself, should impart a yellowish tone. Hence, these data point to the concept of "optical cooperation" between nanoparticles[26,28]–a topic further explored computationally in detail below. Furthermore, since both types of large aggregates produce a similar tone, aggregate size—and less so the degree of coalescence is the primary factor controlling tone. This suggests that a detailed probing of CLS-type aggregates is directly applicable to understanding the microstructure of silver aggregates in photothermographic films.

CLS Conclusions

Beginning with simple, isolated metallic silver nanoparticles in the 5–30 nm diameter range, the following conclusions can be drawn:

- Isolated silver nanoparticles of this size exhibit a yellow tone. As dilute silver particle solutions become more concentrated, the observed change in light absorption (bathochromic shift) properties can be correlated directly to optical cooperation between particles as they begin to aggregate.
- Sufficiently concentrated solutions show significant particle aggregation and ultimately appear black.
- Sufficiently concentrated solutions show an increase in the average component and aggregate particle sizes, indicating that particle coalescence can occur at room temperature.
- Some individual CLS and component particles are found to be single crystals, while others are found to be polycrystalline, which provides the basis for understanding coalescence of silver nanoparticles.
- Concentration induced aggregates show a lower degree of particle fusing than those caused by thermally induced aggregation.

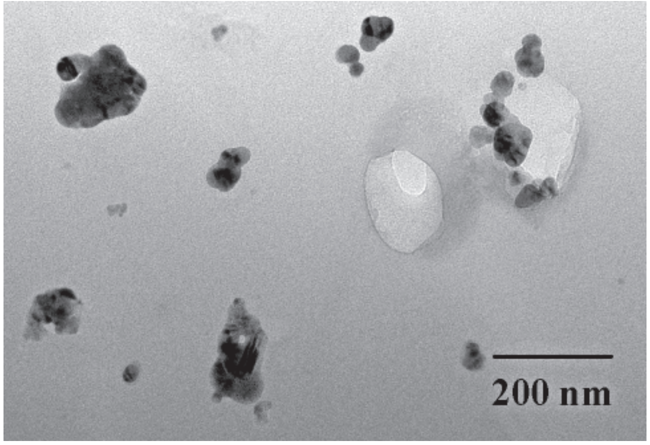

Figure 9. TEM image of silver in the brown CLS film that turned black upon heating to ~200°C.

II. Computational Modeling of Light Absorption by Nanosized silver Particles

Calculating absorption spectra of isolated spherical metallic silver particles, and studying the relationship between size and peak position, can be done directly from the well-known Mie theory.[27] A summary of the application of the Mie theory to photographic emulsions has been provided by Gasper and DePalma (see chapter 20 in Ref. 1). In pioneering work done by Klein and Metz in the early 1960s, a reasonable correlation between the calculated absorption spectra and experimental spectra obtained from silver particles prepared by physical development techniques was observed. The differences

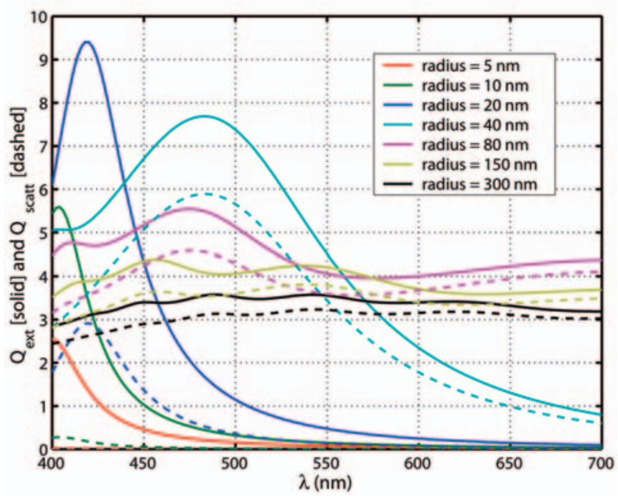

Figure 10. Extinction (solid lines) and scattering (dashed lines) efficiencies of an individual spherical silver particle immersed in a medium with refractive index n = 1.481.

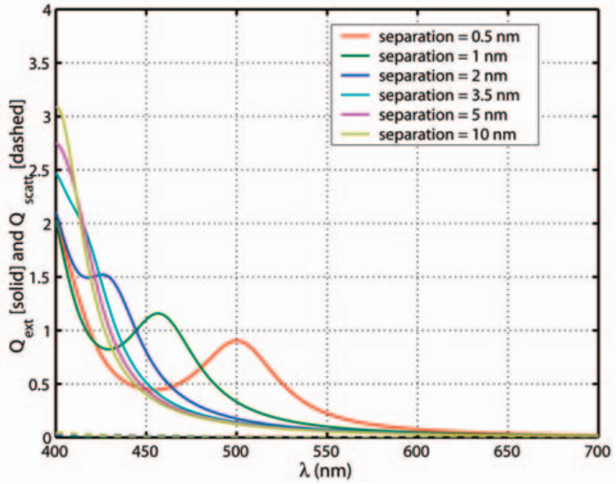

Figure 11. Light extinction (solid lines) and scattering (dashed lines) for a randomly oriented pair of 5 nm radius spherical silver particles immersed in an n = 1.481 medium and separated by the variable distances shown.

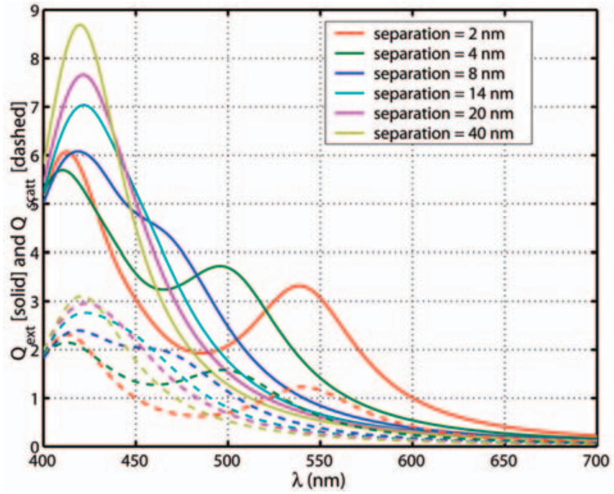

Figure 12. Light extinction (solid lines) and scattering (dashed lines) for a randomly oriented pair of 20 nm radius spherical silver particles immersed in an n = 1.481 medium and separated by the variable distances shown.

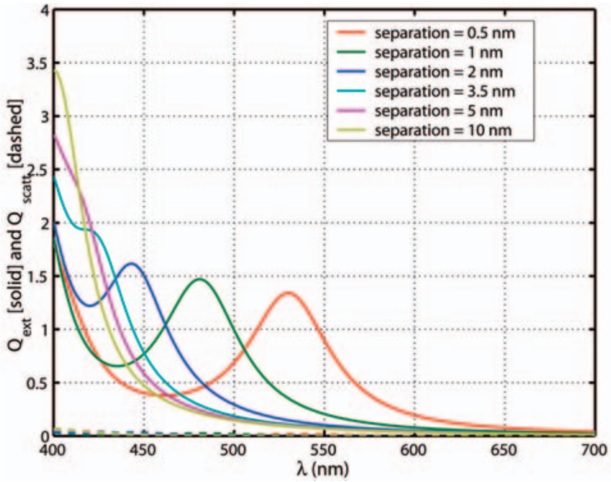

Figure 13. Light extinction (solid lines) and scattering (dashed lines) for a randomly oriented linear chain of three 5 nm radius spherical silver particles immersed in an n = 1.481 medium and separated by the variable distances shown.

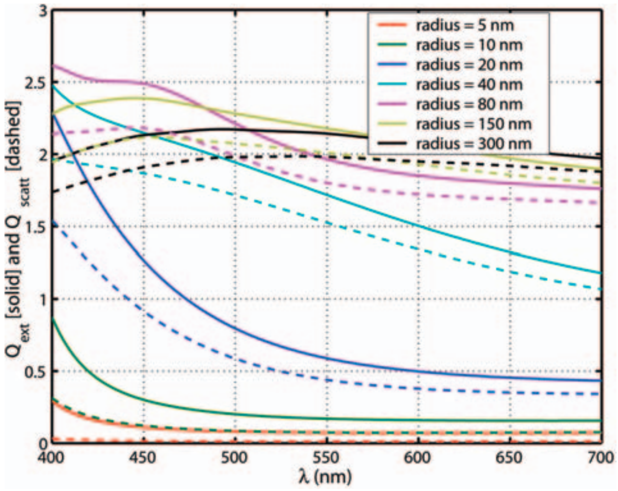

Figure 14. Light extinction (solid lines) and scattering (dashed lines) efficiencies for an isolated metallic silver cylinder, infinite in length, of the radii listed and immersed in an n = 1.481 medium.

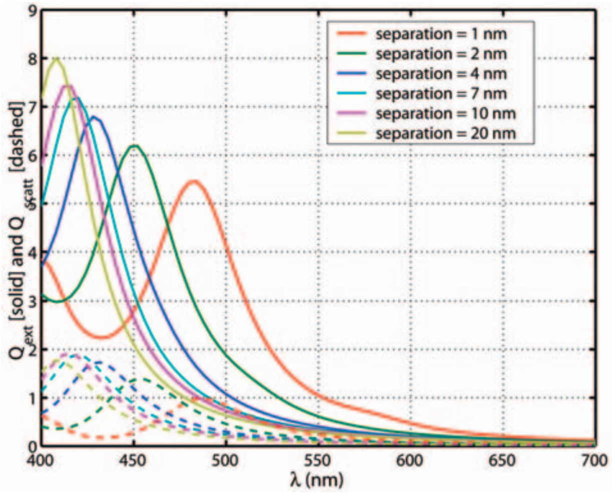

Figure 15. Light extinction (solid lines) and scattering (dashed lines) for a randomly oriented cubic cluster containing eight silver spheres of 10 nm radius immersed in an n = 1.481 medium and separated by the variable distances shown.

were attributed to the deviations from sphericity (because the particles were nearly, but not perfectly, spherical), deviations from monodispersity in the particle size distribution, and deviations in the optical constants of the particles from pure silver as a result of contamination of the silver by adventitious halide.[33] However, the limitations in the calculations themselves, done in a time of rather primitive computational resources, must also be noted: they were performed on a coarse wavelength grid and only over a very limited number of terms in the infinite series that constitutes the Mie solution. There were also errors presumably introduced by the uncertainties in the measured wavelength-dependent optical constants used for silver, which (as Klein and Metz,[33] as well as Bird and coworkers,[34] noted) vary considerably, depending on the source of the measurements. Note also that no attempt was made to correct the optical constants from the bulk values for the finite size of the particles.

In a series of studies,[35–39] Skillman and Berry extended the work of Klein and Metz to include less spherical shapes. They included the effect of the departure from sphericity, as well as the effect of variations in size, refractive index of the silver and the medium, etc. They found, for example, that the absorption spectra of dispersed silver particles are affected more by small departures from the spherical shape than by changes in size or in the refractive index of the medium. They also included many other aspects, such as the optical properties of filamentary silver, concluding, for example, that the optical characteristics of clumps of filamentary silver were quite different than those of a solid sphere of silver having roughly the same outline.

Finally, Bird and co-workers investigated the image tone in diffusion-transfer photographic images. In one paper,[34] they used the Mie theory to study the effect of the contamination of the silver on the resulting tone, assuming that the contamination changed the dielectric constant (and thus the complex refractive index) of the silver by shortening the mean free path of the conduction electrons. In another paper, Jones and Bird[26] studied the effect of aggregation of silver particles on the absorption spectrum; their results provided some evidence that aggregation did cause the tone to become more neutral. However, it is important to note that in order to perform the calculations, they had to make several important simplifying assumptions or approximations. For example, only very specific cluster geometries were considered, namely a linear chain of 2 or 4 equal sized silver particles with light incident from a direction perpendicular to the chain axis and with polarization either parallel or perpendicular to the chain axis. One approximation that they made was to assume the individual particles were small enough, compared to the wavelength of light, that only the lowest order term in the Mie expansion (the electric dipole term) was needed. The second approximation was what they called “the equivalence assumption,” an approximation for how the scattered fields from the particles interact with each other. In that approximation, they assumed that the scattered field from one particle could be assumed to be uniform across the other particles. They noted that this assumption, while good in the limit of well-separated particles, was worse as the particles came closer together, which is, of course, exactly the situation that they were interested in studying. Thus, it is hard to know how broadly those results can be applied. In fact, the results discussed below for linear chains of particles are quite different from those of Jones and Bird, agreeing with their approximate results only in the most basic qualitative sense of also showing a tendency for chains to result in a broader and bathochromically shifted absorption spectrum.

We have proceeded to build on this previous work for application to TG imaging systems, and specifically for nanoparticles in the range observed in the image area of those materials, 5–30 nm diameters, Figs. 2 and 3, the fundamental building block of the dendritic cluster in PTG imaging materials.[3,8–11] The first calculations for isolated spherical silver particles were performed using a code we wrote in MATLAB that implements the Mie theory results.[40] Several Mie codes are also freely available on the web.[41,42] The refractive index of the medium was chosen to be n = 1.481, and the spectrally dependent optical constants for silver were taken from the literature[43,44] and interpolated over the visible spectrum. Next, they were corrected for the finite particle size (and resulting decrease in the mean free path of the conduction electrons) using the approximate formula discussed by Kreibig,[45]

$$\varepsilon(\omega,r)=\varepsilon_{\text{bulk}}(\omega)+\frac{i\omega_p^2 v_F}{\omega^3}\frac{\eta}{r}. \tag{1}$$

where $\varepsilon_{\text{bulk}}$ is the bulk dielectric constant, ω_p is the plasmon frequency, v_F is the Fermi velocity, ω is the (angular) frequency of the light, $i = \sqrt{1}$ denotes the imaginary unit, r is the radius of the particle, and η is a model dependent constant which we take to be 0.5. For silver, $\omega_p = 1.38 \times 10^{16}\ s^{-1}$, $v_F = 1.4 \times 10^6$ m/s.[45] The refractive index is given by $n = \sqrt{\varepsilon}$. This particle size dependent correction to the refractive index produces only modest changes in the quantitative results and has no effect on any qualitative conclusions. The more complicated expression given in Eq. (3) of Ref. 46 reduces to Kreibig’s expression above in the limit $\Gamma << \omega$ which is satisfied for visible light unless $r < 2$ nm. Note that $\gamma_{bulk} = v_F/a_{bulk}$, where the bulk mean free path for silver is $a_{bulk} \cong 55$ nm.

Results of these calculations for isolated single silver particles, of the radii indicated, are given in Fig. 10. Note that the results show both scattering and extinction efficiencies. The latter is the sum of the scattering and absorption efficiencies.

These calculated results correspond well to similar calculations reported by others.[33,38] It can be seen that, as long as the silver particles are separated from each other, the calculated spectrum corresponds well to that of the TEM-observed silver particles, as well as to the UV-visible absorption spectra shown above. How black is obtained from these very same size particles, simply aggregated together, is not clear from these results. It is plausible from Fig. 10 that an aggregation would simply behave like a larger particle. However, one of the main questions then becomes, at what separation distance do the individual particles begin to behave different optically? That is, knowing that isolated particles appear yellow-brown, but agglomerated particles behave roughly as one large particle, and thus appear neutral-black, how does the absorption spectrum begin to exhibit optical cooperation between particles as they come closer together?

The phenomenon of electronic and optical cooperation between nanoparticulate metal particles has been noted in the literature.[26,28] Generally, as the particles come closer together, electronic coupling begins, starting around 5 Å. This can lead to dramatic changes in optical characteristics. The degree of coupling is a function of the particle size and the separation between them. More specifically, and key to the formation of a neutral black absorption, as the separation between particles shortens to physical contact, a new absorption peak appears in the visible region as shown in Fig. 11.

Even at larger separation distances, where electronic cooperation between the particles is negligible, the close proximity of the particles to each other can still have important effects on optical absorption and scattering, provided that the separation distance is on the order of, or smaller than, both the wavelength of light and the diameter of the particles.

The calculation of the optical extinction, absorption, and scattering by a cluster of non-overlapping spherical particles is considerably more complicated and computationally intensive than the Mie calculation for an isolated spherical particle. Nonetheless, with increasing computer power, such computations have become feasible at least for very small clusters.[47–49] Furthermore, FORTRAN codes to perform such calculations have recently been made freely available on the web.[50] We have used these codes, with some modifications to the input and output facilities, to calculate the extinction, scattering, and absorption cross sections of small randomly oriented clusters of silver nanospheres. The same optical constants for silver as for the isolated sphere case were used, except ignoring the correction for the finite size of the particles, since this had been found to have only a small effect.

In the first and simplest case studied, Fig. 11, two 5 nm radius spheres are allowed to approach. The calculated extinction spectrum shows a splitting that begins at a particle separation of nearly 2 nm. The long wavelength peak moves further into the visible region as the separation between the particles becomes smaller. At a separation of 1/10 the radius (0.5 nm, in this case), the peak for this size particle is around 510 nm. Again for a separation of 1/10 the radius, larger particles give the second peak further bathochromically shifted, to ~520 nm for 10 nm radius particles, and ~540 nm for 20 nm radius particles, Fig. 12. Thus, we see a modest bathochromic shift in the second peak as the size of the particles is increased. Note here that we have compared the peak location for different size particles *at a constant ratio of separation distance to radius.* If the peak location for pairs of particles *at a constant value of the separation distance* (such as 2 nm) were compared, the bathochromic shift with increasing particle size would be even more pronounced.

For completeness, the calculated extinction and scattering spectra for 40 and 80 nm radii particles were also studied (not shown), which demonstrated that, as particles become larger, the extinction spectrum becomes more neutral.

When a third particle is included in the calculation, the new absorption peak is shifted further into the visible region, compared to the same-sized pair. For example, the 5 nm radius pair of particles had its peak at ~510 nm (for the 0.5 nm separation), but for three particles, the peak moves to ~530, Fig. 13. Not surprisingly, addition of a fourth particle (not shown here) shifts the peak even further, in this case, to ~550 nm.

As expected, based on the results for isolated particles and for pairs of particles, increasing the particle size for chains of three or more particles simply moves the new peak further into the visible region and broadens it into a more neutral observed color (not shown here).

The physical effect of a fairly long linear collection of particles is also of interest. The calculated spectrum of a linear chain of six 5 nm radius particles suggests that the physical proximity between particles provides the splitting of the absorption band, and different separations between different particles would be expected to provide absorption bands that span the visible spectrum. In order to approximate the case of silver filaments, the optical extinction, absorption, and scattering by randomly oriented infinite-length cylinders of silver having various diameters, Fig. 14, were investigated. As for the cluster calculations, we made use of a computer code that is freely available on the web.[51] Since this code does not perform an average over all orientations of the cylinder, we performed such an average numerically. An infinite cylinder is, of course, only an approximation to the filament geometry, which is not generally straight like the cylinder, and it is clearly not infinite. Comparing the results here to the case of isolated spheres shows a basic similarity in the qualitative features that would determine the general color. In particular, they show an extinction peak in the blue spectrum that flattens out into more uniform extinction as the diameter of the cylinders becomes larger.

There are, however, some notable differences too: for small cylinders, the peak is actually off-scale in the ultraviolet spectrum. Also, there is a less dramatic drop off in the extinction, with increasing wavelength, than for the spheres, with the extinction dropping to a fraction of its peak value and leveling off, rather than dropping off to nearly zero in the green and red, as it does for the small spheres. Finally, as the cylinder size increases, there is no apparent tendency for a well-defined peak to shift to larger wavelengths, i.e., the peak always remains off scale in the ultraviolet; rather, the spectrum just gradually flattens out.

The next most complicated aggregate, a small cluster of eight spherical silver particles arranged in a cubic array, was also calculated. The results for a cluster of 10 nm radius silver particles are shown in Fig. 15. As in the case of just two particles, a peak splitting develops as the particles move closer together. However, unlike in the two-particle case, the higher wavelength peak is the more dominant of the two peaks. Note that this trend toward the higher wavelength peak becoming more dominant was also seen for the case of the chain, as the chain length was made longer.

From all of the TEMs obtained of PTG imaging films, it is clear that the image never contains monodisperse metallic silver particles. Thus, while the above data explain the observed neutral black image in these materials, it is of interest to also consider a calculation for the case of light absorption by two different-sized particles at various separations. Simulations based on this disparity were carried out where two particles of unequal size were brought together. In this case, the smaller particle had radii 5 nm, 10 nm, 20 nm, and 40 nm, and the larger particle was twice as large. The results were quite similar to the results obtained when two equally sized particles were brought together thus demonstrating that the basic conclusions reached here do not depend on all the particles being the same size.

We can define the important optical properties of nanosize metallic silver particles based on literature reports and on our results of the light extinction calculations and CLS TEM/absorption spectral observations as follows:

1. The absorption spectra of spherical silver nanoparticles as a function of their size can be calculated using the Mie theory. As noted previously by others,[33,38] the larger the size, the broader the peak, and the greater the shift into the visible range.

2. Spherical silver nanoparticles begin to absorb light further into the visible when they become physically close to each other.[26,28]
3. Optical cooperation becomes significant when particle separation distance approaches the particle size and smaller. It is important to recognize that the particles do not need to be in direct physical contact to optically cooperate.[26,28]
4. A distribution of spherical silver nanoparticle sizes, when physically close enough to optically cooperate, should be sufficient for neutral black image.
5. Within the distribution of spherical particle sizes, only a few (10–30) optically cooperating nanoparticles would be needed for efficient light absorption to obtain a black image. This minimum number requires a distribution of individual particle sizes, ranging from 5–30 nm, and separations, from physical contact up to multiple nm.
6. Isolated silver nanoparticles in images contribute to poor image tone (yellow) as well as poor silver efficiency.

Conclusions

Using a combination of fundamental investigations of nanosilver particles with theoretical light absorption calculations and direct correspondence to imaging materials, we have demonstrated the underlying principles to achieving optimum light absorption by the metallic silver in photothermographic imaging systems. Specifically, the fundamental building blocks of color are spherical 5–30 nm diameter nanoparticles of silver, and while the size and shape of silver particles are important factors that affect the image optical density and tone, silver particle physical proximity that results in optical cooperation is just as important. Moreover, we can further say that the filamentary shape is an inefficient use of silver, compared to any other shape, spherical, oblate, etc. Consequently, for photothermographic, as well as thermographic, imaging systems, the optimum silver for the highest optical density, with a neutral tone, of a black-and-white image using the least amount of silver, can now be defined:

1. The silver particles must be in the nano range of 5–30 nm. Larger particles are an inefficient use of silver.
2. The silver particle size must be polydisperse in order to produce a wide variety of absorption peaks throughout the visible region.
3. The silver nanoparticles must be agglomerated (isolated silver nanoparticles constitute yellow CLS).
4. The optimum optical cooperation between silver particles occurs when the nanoparticles are separated by much less than the particle size.
5. The separation between silver particles should preferably comprise polydisperse distances, which provides a polydisperse set of absorption peaks throughout the visible spectrum.

In other words, the ideal silver for achieving a neutral black image with the least amount of silver is an aggregation consisting of 10–30 extremely fine (5–30 nm diameter), but polydisperse, nanoparticles of metallic silver. The minimum aggregation size should be in the 50–200 nm diameter range, depending on the aggregate shape. These are exactly the types of metallic silver dendrites component that are observed in PTG imaging systems.[3,4,8–11]

Acknowledgments. We are indebted to R. DeKeyzer (Agfa) for bringing the G. Bird references to our attention and to R. J. Meyer (Eastman Kodak Company) for selected microtomy and TEM image capture.

References

1. T. H. James, *The Theory of the Photographic Process*, 4th ed., (Macmillan, New York, NY, 1977), p. 390.
2. W. Van Renterghem, D. Schryvers, J. Van Landuyt, C. Van Roost, and R. De Keyzer, *J. Imaging Sci. Technol.* ISSN: 1062-3701, **47**, 133 (2003).
3. D. R. Whitcomb, “Photothermographic and Thermographic Imaging Materials,” in *Kirk Othmer Encyclopedia of Chemical Technology*, online edition, 2003, http://www3.interscience.wiley.com/cgi-bin/mrwhome/104554789/HOME.
4. P. Cowdery-Corvan and D. R. Whitcomb, “Photothermographic and Thermographic Imaging Materials”, in *Handbook of Imaging Materials,* A. Diamond and D. Weiss, Eds. (Marcel Dekker, New York, NY, 2001), p. 473.
5. D. H. Klosterboer, in *Neblette’s Eighth Edition*: *Imaging Materials and Processes*, J. M. Sturge, V. Walworth and A. Shepp, Eds., (Van Nostrand-Reinhold, New York, NY, 1989), chap. 9, pp. 279–291.
6. M. R. V. Sahyun, *J. Imaging Sci. Technol.* ISSN: 1062-3701, **42,** 23 (1998).
7. S. E. Hill, M. B. Mizen, M. R. V. Sahyun, and Yu. E. Usanov, *J. Imaging Sci. Technol.* ISSN: 1062-3701, **40**, 568 (1996).
8. B. B. Bokhonov, L. Burleva, Yu. Usanov, and D. R. Whitcomb, *J. Imaging Sci. Technol.* ISSN: 1062-3701, **45**, 259 (2001).
9. B. B. Bokhonov, L. P. Burleva, W. Frank, M. B. Mizen, M. R. V. Sahyun, D. R. Whitcomb, J. Winslow, and C. Zou, *J. Imaging Sci. Technol.* ISSN: 1062-3701, **40** (1996) 417.
10. B. B. Bokhonov, L. P. Burleva and D. R. Whitcomb, *J. Imaging Sci. Technol.* ISSN: 1062-3701, **43**, 505 (1999).
11. B. B. Bokhonov, L. P. Burleva, Yu. E. Usanov, and D. R. Whitcomb, *Zh. Nauchn. Prikl. Fotogr.* **44,** 11 (1999).
12. T. Ohzeki, Y. Yoshioka and K. Nagao, *Proc. IS&T/SPSTJ Int’l. Symp. Silver Halide Technol.,* (IS&T, Springfield, VA, 2004), p. 7.
13. M. de Clerck, *Proc. Int. Conf. Imaging. Sci.*, *ICPS ’98*, (KVCV, Antwerp, Belgium, 1998), p. 106.
14. S. Emmers, B. Horsten, I. Geuens, Y. Gilliams, A. Bellens, D. Bollen, and I. Hoogmarten, US Patent No. 6,159,667 (2000).
15. C. Uyttendaele, H. Uytterhoeven and B. Horsten, EP 692,733 (1998).
16. B. B. Bokhonov, L. P. Burleva, D. R. Whitcomb, and M. R. V. Sahyun, *Microsc. Res. Tech.* **42**, 152 (1998).
17. M. C. Lea, *J. Amer. Sci.* **33** 476 (1889).
18. M. Faraday, *Philos. Trans. R. Soc.* Lond. **147**, 145 (1857).
19. J. Turkevich, P. C. Stevenson and J. Hillier, *Disc. Faraday Soc.* **11** 55 (1951).
20. J. M. Thomas, *Pure Appl. Chem.* **60**, 1517 (1988).
21. L. Stroebel, J. Compton, I. Current, and and R. Zakia, *Basic Photographic Materials and Processes*, (Focal Press, Boston, MA, 2000), p. 314.
22. M. Kerker, O. Silman, L. A. Bum, and D.-S. Wang, *Appl. Optics*, **19**, 3253 (1980).
23. H. Wetzel, H. Gerischer and B. Pettinger, *Chem. Phys. Lett.* **85**, 187 (1982).
24. J. H. Schott and H. S. White, *J. Phys. Chem.* **98**, 297 (1994).
25. M. Kawasaki and H. Ishii, *Langmuir*, **11**, 832 (1995).
26. R. C. Jones and G. R. Bird, *Photogr. Sci. Eng.* **16**, 16 (1972).
27. G. Mie, *Ann. Phyzik.* **25**, 377 (1908).
28. C. B. Murray, C. R. Kagan and M. G. Bawendi, *Ann. Rev. Mater. Sci.* **30**, 645 (2000).
29. V. V. Sviridov, G. A. Branistky, O. V. Sergeyeva, V. D. Stashonok and L. P. Rogach, *J. Inf. Rec. Mater.* **20**, 345 (1993).
30. V. D. Stashonok, O. V. Sergeeva, M. V. Artemev, V. I. Grigorenko, *Zhur. Nauch. i Prikl. Photogr. i Kinematogr.* **35**(4) 280 (1990).
31. V. V. Sviridov, G. A. Branitzki, O. V. Sergeeva, V. D. Stashonok, M. V. Artemev, and L. P. Rogach, *Zhur. Nauch. i Prikl. Photogr. i Kinematogr.* **33**(1), 71 (1988).
32. P. V. Kamat, *J. Phys. Chem.* B, **106**, 7729 (2002).
33. K. Klein and H. J. Metz, *Photogr. Sci. Eng.* **5,** 5 (1961).
34. G. R. Bird, M. Morse, H. Rodriguez, P. E. Bastian, J. Johnson, and W. E. Gray, *Photogr. Sci. Eng.* **15**, 356 (1971).
35. D. C. Skillman and C. R. Berry, *J. Chem. Phys.* **48**, 3297 (1968).
36. C. R. Berry and D. C. Skillman, *J. Photogr. Sci.* **17**, 145 (1969).
37. C. R. Berry and D. C. Skillman, *Photogr. Sci. Eng.* **15**, 236 (1971).
38. D. C. Skillman and C. R. Berry, *J. Opt. Soc. Amer.* **63**, 707 (1973).
39. D. C. Skillman, *Photogr. Sci. Eng.* **19**, 28 (1975).
40. P.W. Barber and S.C. Hill, *Light Scattering By Particles: Computational Methods*, (World Scientific, Singapore, 1990), chap. 4.
41. T. Wriedt, Electromagnetic Scattering Programs, University of Bremen, website, http://www.iwt-bremen.de/vt/laser/wriedt/index_ns.html
42. P. J. Flatau, SCATTERLIB Light Scattering Codes Library, University of California at San Diego, website, http://atol.ucsd.edu/~pflatau/scatlib/
43. H.-J. Hagemann, W. Gudat, and C. Kunz, *Optical Constants From the*

Far Infrared to the X-Ray Region: Mg, Al, Cu, Ag, Bi, C, and Al_2O_3, DESY SR-74/7, Hamburg, AG, 1974.
44. *CRC Handbook of Chemistry and Physics*, D. R. Lide, Ed., (CRC Press, Boca Raton, FL, 2003).
45. U. Kreibig, *Z. Phys. B,* **31**, 39 (1978).
46. R. D. Averitt, D. Sarkar and N. J. Halas, *Phys. Rev. Lett.* **78**, 4217 (1997).
47. M. I. Mishchenko, *J. Opt. Soc. Amer.* A, **8**, 871 (1991).
48. D. W. Mackowski, *J. Opt. Soc. Amer.* A, **11**, 2851 (1994).
49. M. I. Mishchenko and D. W. Mackowski, *Opt. Lett.* **19**, 1604–1606 (1994).
50. Code "scsmtm1.for" written by D. W. Mackowski, K. Fuller, and M. L. Mishchenko, and code "bisphere.f" written by M. L. Mishchenko and D. W. Mackowski, both are available at http://www.giss.nasa.gov/~crmim/t_matrix.html
51. Code "cylm.for" written by D. W. Mackowski and is available at http://atol.ucsd.edu/~pflatau/scatlib/